Electrochemiluminescent detection of epilepsy biomarker miR-134 using a metal complex light switch

Robert J Forster, David C Henshall, Hany El Naggar, Yann Pellegrin, Norman Delanty

Bioelectrochemistry 146 (2022) 108150

Contents lists available at ScienceDirect

Bioelectrochemistry

journal homepage: www.journals.elsevier.com/bioelectrochemistry

Electrochemiluminescent detection of epilepsy biomarker miR-134 using a metal complex light switch

Robert J. Forster [a,*], David C. Henshall [b], Hany El Naggar [c], Yann Pellegrin [d], Norman Delanty [c]

[a] National Centre for Sensor Research, School of Chemical Sciences, Dublin City University, Dublin 9, Ireland. FutureNeuro, The SFI Research Centre for Chronic and Rare Neurological Diseases, Ireland
[b] FutureNeuro, The SFI Research Centre for Chronic and Rare Neurological Diseases, RCSI, University of Medicine and Health Sciences, Dublin, Ireland
[c] The National Epilepsy Programme, Beaumont Hospital, Dublin, Ireland, FutureNeuro, The SFI Research Centre for Chronic and Rare Neurological Disease, Dublin, Ireland, The Royal College of Surgeons in Ireland, Dublin, Ireland
[d] Université de Nantes, CEISAM, UMR CNRS 6230 UFR Sciences and Techniques, Nantes, France

ARTICLE INFO

Keywords:
Electrochemiluminescence
Ruthenium luminophore
miRNA
Electrochemical biosensor
Epilepsy biomarker

ABSTRACT

The detection of a key biomarker in epilepsy, miR-134, using an environmentally sensitive electrochemiluminescent luminophore, $[Ru(DPPZ)_2\ PIC]^{2+}$, is reported, DPPZ is dipyrido[3,2-a:2′,3′-c]phenazine) and PIC is (2,2′-bipyridyl)-2(4-carboxy phenyl) imidazo [4,5][1,10] phenanthroline. A thiolated capture strand is first labelled with $[Ru(DPPZ)_2\ PIC]^{2+}$ and then adsorbed onto a gold electrode. No significant electrochemiluminescence, ECL, is observed for immobilised Ru-labelled capture strands which is consistent with the light-switch dye being exposed to the aqueous solution. In sharp contrast, binding of the target turns on ECL. The ECL intensity, I_{ECL}, depends on the number of adenine "spacer" bases between the end of the capture sequence and the dye. The ECL intensity for the optimised system increases linearly with increasing miR-134 concentration from 100 nM to approximately 20 μM. Single and double base mismatches produce I_{ECL} that are only approximately 30% and 8% respectively of that observed for the fully complementary target reflecting differences in their association constants. Significantly, the presence of BSA protein causes I_{ECL} to increase by less 5% in either the single or duplex circumstances. Finally, the ability of the sensor to quantify miR-134 in unprocessed plasma samples from healthy volunteers and people with epilepsy is reported.

1. Introduction

Around 50 million people worldwide have epilepsy, making it one of the most common neurological diseases globally [1,2]. The primary tool used for diagnosis of seizure disorders is the electroencephalogram (EEG) [3,4] which is technically demanding to interpret and can have a relatively low clinical sensitivity due to people with epilepsy showing normal EEGs while medically normal individuals can show abnormal EEG results [5]. MicroRNAs, miR, are emerging as a high impact class of biomarkers for the diagnosis and monitoring of a broad range of diseases [6] including epilepsy [7,8,9,10]. These short strands of nucleic acids (20–25 bases) are noncoding and regulate protein levels in cells by post-transcriptional interference in gene expression. In epilepsy, miR-134 is selectively enriched in specific brain cell types and it modulates interneuronal signalling by interacting with proteins that influence dendrite formation [11,12]. Upregulation of miR-134 in rodent models of status epilepticus and human epilepsy, [13] reveal that silencing miR-134 can help to suppress seizures in mice [14]. There is also evidence that some miRNAs are at a higher concentration in blood following seizures and even prior to seizures in rodents, [15] and in epilepsy patients [16]. Moreover, miR-134 represents an attractive, druggable target [17,18]. The ability to predict an impending seizure through a blood test would revolutionise the lives of people with epilepsy, but traditional approaches, such as qPCR, have long turnaround times and are challenging to implement at the point-of-need. Therefore, there is a critical unmet need for novel sensors to sensitively detect the systemic concentration of key miRNA to enable data driven clinical decision making and to enable patients to monitor their own health outside of the clinic. Electrochemical sensors have particular advantages in terms of their low cost, portability and multianalyte capabilities [19]. However, the concentration of the miRNA can be as low as picomolar requiring highly sensitive detection strategies such as electrocatalysis to amplify

* Corresponding author.
E-mail address: Robert.Forster@dcu.ie (R.J. Forster).

https://doi.org/10.1016/j.bioelechem.2022.108150
Received 24 March 2022; Received in revised form 27 April 2022; Accepted 28 April 2022
Available online 5 May 2022

the signal rather than the target concentration, [20,21,22,23,24,25] or the use of complex, high-cost microfluidic devices [26]. Electrochemiluminescence [27,28,29,30,31,32] can enable highly sensitive detection because the background is dark (ultimately the limit of detection is controlled by the signal to noise ratio) and diverse strategies to enhance response have been identified [33,34,35,36,37].

As shown in Scheme 1, in this contribution we report on the direct detection of miR-134 using an environmentally sensitive metal complex, $[Ru(DPPZ)_2\ PIC]^{2+}$, whose electrochemiluminescence is turned on when intercalated within the duplex that forms when the target is present.

This "light switch" capability simplifies the assay design since the luminophore can be coupled to the capture sequence and immobilised on the gold electrode surface, but it does not generate ECL until the capture-target duplex is formed. Unlike other approaches that use a three-strand configuration, i.e., capture-target-labelled probe, which requires two distinct hybridisation as well as wash steps, here, only a labelled capture strand is needed, and washing can be minimised because ECL is turned on only when the duplex forms. New approaches to the synthesis of DPPZ based luminophores and their conjugates [38,39] have been devised and used previously for the electrochemiluminescent detection of diverse analytes including Hg^{2+}, [40] ATP, [41] DNA from pathogens, [42] N-acetyl-β-d-glucosaminidase, [43] amyloid-β oligomerization, [44] miRNA, [45,46] among others, as well as elucidating the interaction of small molecules and DNA [47] ECL generation requires the luminophore to intercalate into the duplex which requires some flexibility. To investigate this issue, "spacer" adenine bases have been inserted between the complementary target binding region and the dye attachment point. Significantly, while ECL is observed for each system following hybridisation of the target, the optimal spacer length shows an ECL intensity that is approximately five times higher than that observed in the absence of a spacer. This result suggests that giving the luminophore additional flexibility enhances its ability to intercalate. Using the optimum spacer length, the ECL intensity depends linearly on the miR-134 concentration from approximately 0.1 to 25 μM. Significantly, the presence of proteins such as bovine serum albumin, BSA, at physiologically relevant concentrations does not turn on ECL in the absence of the target and the ECL intensity when miR-134 is bound is less than 5% higher when BSA is present. The presence of a single and double base mismatches causes the ECL intensity to decrease by approximately 70% and 92%, respectively, relative to the fully complementary target. Finally, the ECL responses before and after washing are within 7% of one another suggesting that the assay can be simplified by eliminating the final wash step.

2. Experimental

2.1. Microelectrodes

For high-scan rate voltammetry, microelectrodes were prepared using 25 μm radius gold microwires sealed in a glass shroud that were mechanically polished as described previously [48]. Electrochemical cleaning of the electrodes was carried out by cycling in 0.1 M H_2SO_4 between potential limits chosen to initially oxidize and then reduce the surface of the gold electrode. Excessive cycling was avoided in order to minimize the extent of surface roughening. The real surface area of the electrodes was determined by calculating the charge under the gold oxide reduction peak. Typically, surface roughness values were between 1.4 and 1.8. Determining the real, as opposed to the geometric area of the electrodes is important if the area of occupation of the adsorbate is to be accurately determined.

2.2. Instrumentation

Cyclic voltammetry was performed using a CH Instruments Model 660 Electrochemical Workstation and a conventional three electrode cell. All solutions were degassed thoroughly using nitrogen, and a blanket of nitrogen was maintained over the solution during all experiments. Potentials are quoted with respect to a CH Instruments Ag/AgCl reference electrode filled with saturated KCl which had a potential of + 0.190 V with respect to the normal hydrogen electrode and was connected to the cell via a salt bridge. All experiments were performed at room temperature (22 ± 3 °C).

2.3. Nucleic acid assay

The oligonucleotides were purchased from Eurogentec (98 %), Belgium. The capture probe was a 3′ thiol, 5′ amino modified oligonucleotide:

Capture: NH_2– 5′-ACC-AGU-CAC-A-3′-SH;

Target (miR-134): 5′-UGU-GAC-UGG-UUG-ACC-AGA-GGG-G-3′;

1-base mismatch (miR-758): 5′-UGU-GAC-UGG-UUG-ACC-AGA-GAG-G-3′;

The metal complex was synthesized and characterised as reported previously, [49] and used to label the capture strand in two steps. First, Ru $(DPPZ)_2$ PIC was dissolved in DMSO with a molar equivalent of sodium-4-((4-(cyanoethynyl)benzoyl)oxy)-2,3,5,6-tetrafluorobenzenesulfonate (CBTF) and stirred for approximately 10 min at room temperature. A molar equivalent aliquot was then added to

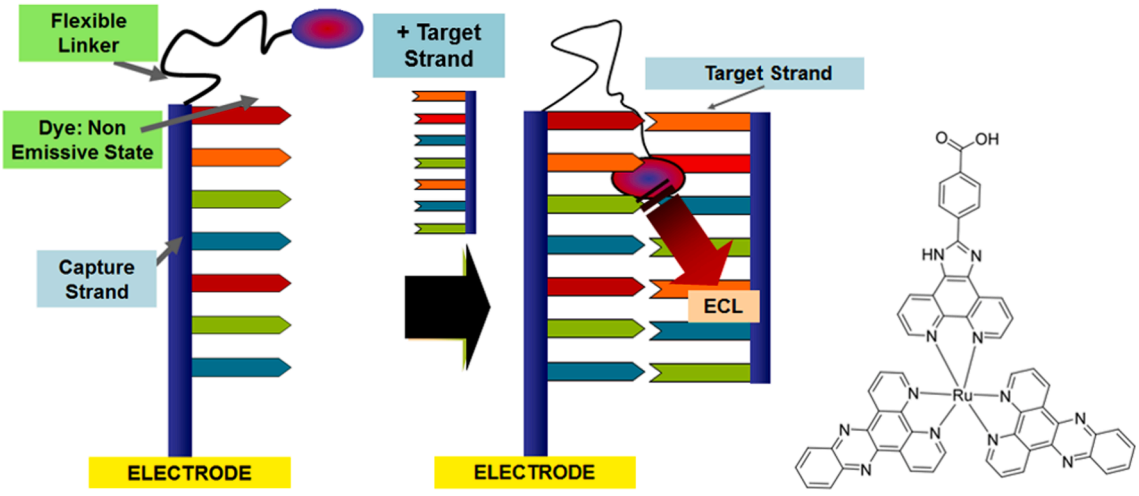

Scheme 1. Schematic representation of the detection of miR-134. The Ru-DPPZ based luminophore is not ECL active when in water, but upon hybridisation of the target to form a duplex, the luminophore can intercalate turning on ECL. The emission intensity is proportional to the quantity of miR-134 that is bound.

the amino terminated NA capture probe strand in PBS (pH 7.4) and stirred for a minimum of 60 min. The Ru-probe NA was purified using the QIAquick® PCR Purification Kit (Qiagen, Valencia, CA, USA) using the manufacturer's protocol. The NA was eluted in water or 1 mM Tris-HCl buffer, pH 8.5. The modified NA was precipitated with the addition of 0.1 vol of 3 M sodium acetate, pH 5.2, and 2 volumes of absolute ethanol.

Denhardt's Hybridisation solution (≥99.5%) was used for DNA immobilisation and hybridisation and was used as received from Sigma Aldrich. The gold (micro)electrodes were functionalised with the capture strands by immersing in a 1 μM solution of the Ru modified, thiolated capture NA in Denhardt's solution for 14 h at 37C. The microelectrodes were then repeatedly (5 x) immersed, washed with buffer and then soaked in buffer for 20 min to remove any unbound material. Hybridization of the target DNA strand to the capture strand was performed at 37 °C for 30 min.

2.4. Human plasma samples

All studies involving human subjects and samples were approved by the Research Ethics Committee of the Royal College of Surgeons in Ireland (RED #859) and by the Ethics (Medical Research) Committee of Beaumont Hospital, Dublin. Informed written consent was obtained from all patients and volunteers. Blood was collected by venepuncture into K2-EDTA tube, 10 ml, BD cat. No. 367525, gently inverted 8–10 times, and processed to obtain plasma within one hour. Plasma was prepared by centrifuging the tubes at 1300 g, for 10 mins at 4 °C. A second centrifugation step was performed at 1940 × g for 10 min at 4 °C to further reduced cellular contamination [50]. After centrifugation, samples were decanted for storage in a cryo-tube (Greiner Bio-one) and frozen at − 80 °C.

Plasma was obtained from two healthy volunteers (female, 38; male, 25) and four temporal lobe epilepsy patients attending the video EEG monitoring unit at Beaumont hospital for epilepsy diagnosis. All patients were on medication at the time of the study.

3. Results and discussion

3.1. General electrochemical properties

Fig. 1 shows representative background corrected cyclic voltammograms for the $Ru^{2+/3+}$ couple within a spontaneously adsorbed film of the thiolated miR capture strand labelled with the $[Ru(DPPZ)_2\ PIC]^{2+}$. The electrolyte is aqueous 1.0 M $LiClO_4$. The voltammetric peak heights change by less than 10% when the monolayer is repeatedly cycled for periods up to 2 h in blank electrolyte solutions.

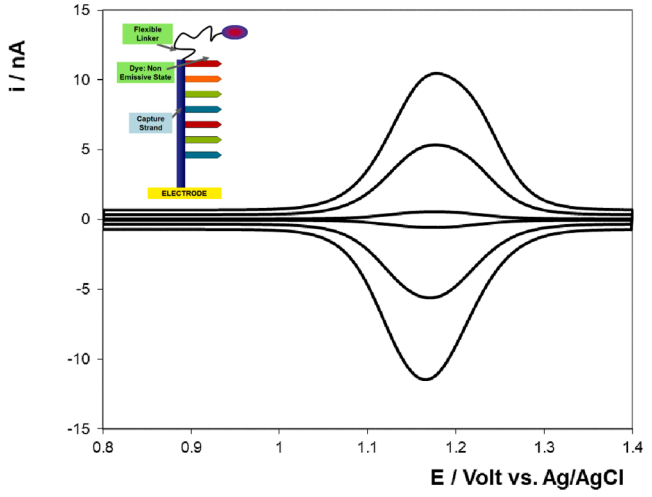

Fig. 1. Scan rate dependent, background corrected, cyclic voltammograms of the miR-134 capture-monolayer covalently labelled with $[Ru(DPPZ)_2\ PIC]^{2+}$. The electrolyte is 1.0 M $LiClO_4$. The electrode is a gold disk with a 25 μm radius and a surface roughness of 1.6. The surface coverage, Γ, is 0.34 ± 0.05 × 10^{-10} mol cm^{-2}. From top to bottom, the scan rates are 10, 5, and 1 V s^{-1}.

These voltammograms are consistent with those expected for an electrochemically reversible reaction for the surface-confined species $Ru^{2+/3+}$ couple with a formal potential, $E^{o'}$, of 1170 ± 10 mV [51,52]. The peak shape is independent of scan rate, υ, for $0.5 \leq \upsilon \leq 10$ V s^{-1} and the peak height increases linearly with increasing scan rate, rather than the $\upsilon^{1/2}$ dependence observed for the complex in solution. The peak-to-peak separation, ΔE_p, even at 10 V s^{-1} is only 12 ± 3 mV. Fitting the scan rate dependent voltammograms ($50 \leq \upsilon \leq 100$ V s^{-1}) indicates that k^o is 5.3 ± 0.8x10^{-1} s^{-1}. This value is significantly lower than that found for structurally related systems that have a shorter electron transfer distance, e.g., k^o for $[Ru(bpy)_2(bpySH)](PF6)_2$ is 0.9 ± 0.1x10^4 s^{-1}, where bpy is 2,2′-bipyridyl and bpySH is 5,5′-bis(mercaptomethyl)-2,2′-bipyridine [53]. However, given that the length of the single RNA strand is of the order of 7–8 nm, and k^o decreases exponentially with increasing distance, the rather large k^o observed suggests that the capture strand may not be fully extended. The full width at half maximum current is 125 ± 20 mV indicating that there are weak destabilizing interactions between the adsorbates. Integrating the charge passed indicates that the surface coverage is 3.4 ± 0.1x10^{-11} mol cm^{-2} using the real surface area which corresponds to an area per dye molecule of 440 $Å^2$. The surface coverage is significantly less than that expected where the metal complexes are close-packed (≈1x10^{-10} mol cm^{-2}). If the adsorbates are uniformly distributed across the electrode surface, i.e., the RNA capture strands do not form islands, they would be separated by approximately 8 nm which leaves sufficient space for the target to hybridise and for the dye to intercalate within the duplex formed when the target hybridises.

3.2. Effect of target hybridization on the voltammetry

Hybridisation is expected to cause changes in the layer structure that could affect the voltammetric response. For example, formation of a duplex should rigidify the structure and lead to a more extended configuration of the RNA strand increasing the electron transfer distance and giving a lower rate of heterogeneous electron transfer. More significantly, the $[Ru(DPPZ)_2\ PIC]^{2+}$ dye is expected to intercalate within the duplex through the phenazine ligand, changing its local microenvironment which might affect the oxidation or reduction potentials. Fig. 2 shows voltammograms at 10 V s^{-1} before and after hybridisation using a 50 μM solution of the miR-134 target. A high target concentration was used to maximise the formation of the duplexes into which the dye can intercalate.

Even at 0.5 V s^{-1}, ΔE_p increases from 12 ± 3 mV to 71 ± 5 mV following miR-134 hybridisation suggesting a significantly lower k^o. Significantly, the anodic peak shifts in a positive potential direction by 35 ± 5 mV indicating that it is thermodynamically more difficult to create the Ru^{3+} centres which is consistent with metal complex being intercalated within the duplex. The anodic peak also broadens with a FWHM of 155 ± 5 mV and develops a distinct shoulder perhaps suggesting that there may be more than one type of binding site, e.g., different physical locations for intercalation within the duplex, or the capture strands themselves may exist as isolated adsorbate and within densely packed islands.

3.3. Electrochemiluminescence properties

In the presence of co-reactants such as tripropyl amine or oxalate, radicals are electrogenerated that can chemically reduce the electrogenerated Ru^{3+} leading to a significant electrocatalytic current. Fig. 3A shows voltammetry in the presence of 10 mM oxalate as co-reactant before and after hybridisation of the miR-134 target. In both cases, a significant catalytic current is observed with peak potentials of 1.22 V

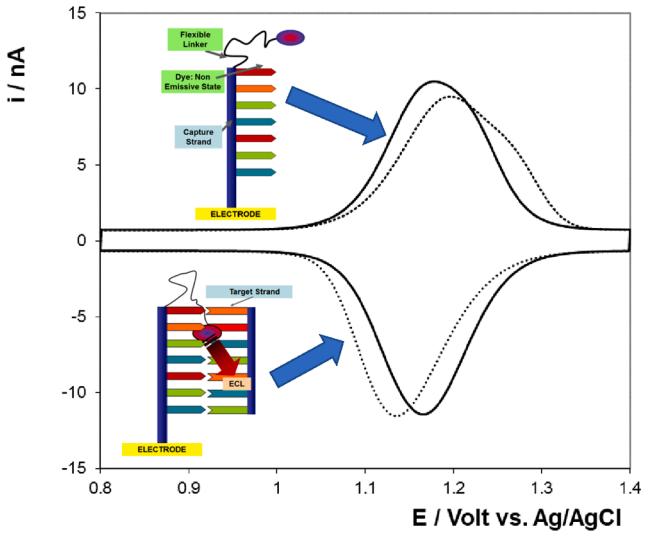

Fig. 2. Voltammetry of a miR-134 capture-$[Ru(DPPZ)_2\ PIC]^{2+}$ monolayer in 1.0 M aqueous $LiClO_4$. pH 6.9 before (solid line) and after (dashed line) exposure to a 50 μM solution of target miR-134 for 30 min. The scan rate is 10 Vs^{-1}. The electrode is a gold disk with a 25 μm radius and a surface roughness of 1.6. The surface coverage, Γ, is 0.34 ± 0.05 × 10^{-10} mol cm^{-2}.

and 1.30 V, respectively, and the current magnitudes are within 20% of one another. These results demonstrate that the ruthenium complex is accessible to the co-reactant in both the single and double stranded RNA forms and that at slow scan rates, intercalation of the metal complex does not significantly impact the generation of the potentially emissive Ru^{2+*} state.

However, Fig. 3B shows that hybridisation of the target has a dramatic effect on the magnitude of the electrochemiluminescence with the intensity of the ECL observed after target binding being approximately *400 times larger* than that observed for the single stranded RNA despite the fact that the electrocatalytic currents are similar in both circumstances (Fig. 3A). These data demonstrate that only Ru^{2+*} centres that are intercalated within double stranded microRNA can generate ECL. When the target is not hybridised, the excited states interact with the aqueous solvent and relax to the ground state without the emission of light. This finding opens the possibility of simplified and highly sensitive detection of miRNA, i.e., labelled capture strand binding the target rather than the capture-target-labelled probe strand configuration of conventional assays. It may also enable a wash-free assay which is considered later.

The intercalation of the dye requires physical movement of the tethered dye which may be influenced by the length of the linker between the end of the RNA capture sequence and the dye itself. To address this issue, we have created thiolated capture strands that incorporate 0, 3, 6, 9 or 12 adenine spacer groups between the fully complementary capture sequence and the dye. These bases do not hybridise with the target and are intended to enhance the flexibility of the dye linkage to allow deeper intercalation which protects the excited state from quenching by water molecules. Fig. 4 shows the dependence of the ECL intensity generated from the $[Ru(DPPZ)_2\ PIC]^{2+}$ on the number of adenine spacer groups. The electrocatalytic current observed is independent of the number of spacer bases to within 20%. Significantly, the ECL intensity increases substantially with an increasing number of spacer groups up to nine adenine bases. The association constant for the binding of the miR-134 target is expected to be independent of the number of spacer bases since the capture sequence is unchanged. The increase in ECL intensity arises because the increased flexibility of the longer spacers facilitates intercalation of the environmentally sensitive $[Ru(DPPZ)_2\ PIC]^{2+}$ dye reducing the fraction of excited states that are deactivated by contact with the aqueous solution. The observation that nine and 12 spacers give statistically indistinguishable intensities suggests that these spacers are sufficiently flexible to maximise intercalation and protection of the luminophore. Therefore, the following investigations were carried out using a capture strand with 9 adenine spacers between the end of the sequence complementary to the target and the ruthenium dye.

Fig. 5 shows the dependence of the ECL response on the electrode voltage where the capture strands have been hybridised with different concentrations of the miR-134 target between 100 nM and 100 μM. Consistent with the voltammetry shown in Fig. 2, the ECL response shows a shoulder at more positive potentials that dominates the response for the higher concentrations of the miR-134 target. This result suggests that there may be more than one type of binding site or microenvironment for the DPPZ dye within the duplex formed in the presence of the target. The inset of Fig. 5 shows the dependence of the fraction of the ECL luminophore that is bound within the duplex, θ, and hence generates ECL, as a function of the target concentration. The quality of the best fit to these experimental data using a single binding site model is poor and to probe this issue further the Hill model, Equation (1), describing cooperative binding at n different binding sites was used:

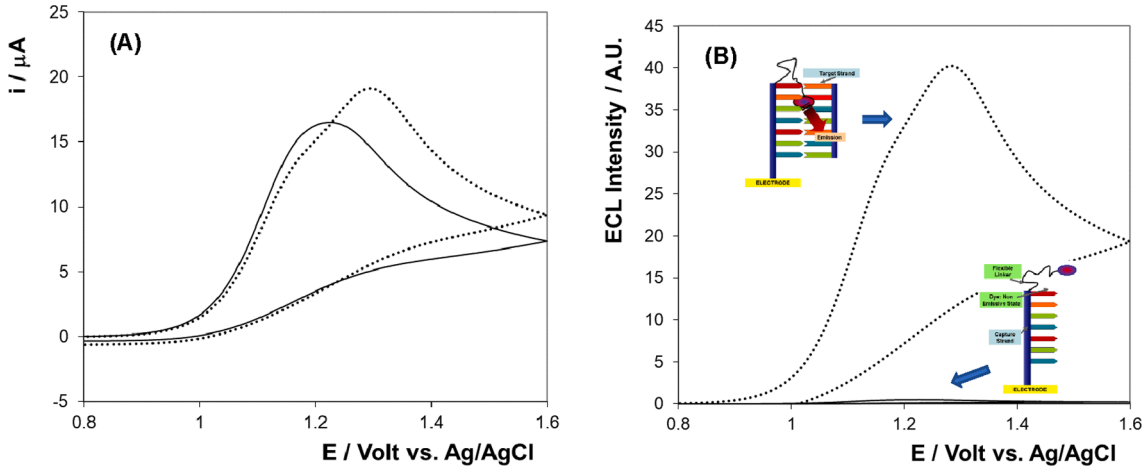

Fig. 3. (A) Current response of a miR-134 Capture-$[Ru(DPPZ)_2\ PIC]^{2+}$ monolayer immersed in in 1.0 M $LiClO_4$ containing 10 mM oxalate as co-reactant before (solid line) and after (dashed line) exposure to a 50 μM solution of miR-134. (B) ECL from miR-134 Capture-$[Ru(DPPZ)_2\ PIC]^{2+}$ monolayer in 1.0 M $LiClO_4$ containing 10 mM oxalate as co-reactant before (solid line) and after (dashed line) exposure to a 50 μM solution of miR-134. For both A and B, the scan rate is 0.1 Vs^{-1}. The electrode is gold deposited on silicon, area 0.09 cm^2. The surface coverage, Γ, is 0.34 ± 0.05 × 10^{-10} mol cm^{-2}.

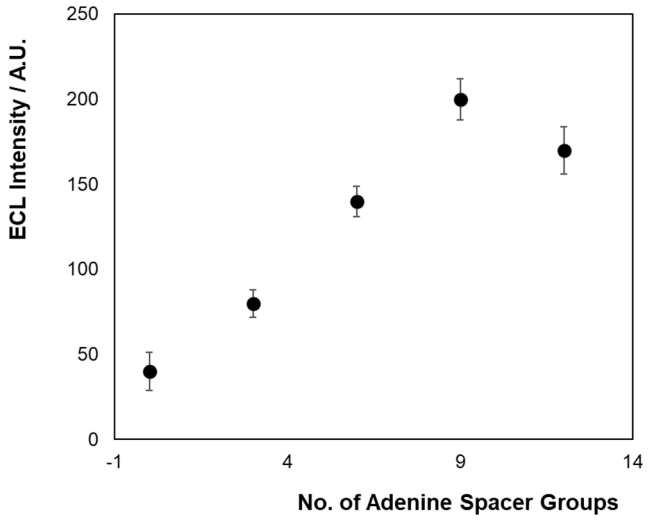

Fig. 4. Dependence of the ECL intensity on the number of adenine spacer groups between the end of the miR-134 capture sequence and the $[Ru(DPPZ)_2PIC]^{2+}$ dye. The miR-134 target concentration is 50 μM. The co-reactant is 10 mM oxalate and the supporting electrolyte is 1.0 M aqueous $LiClO_4$.

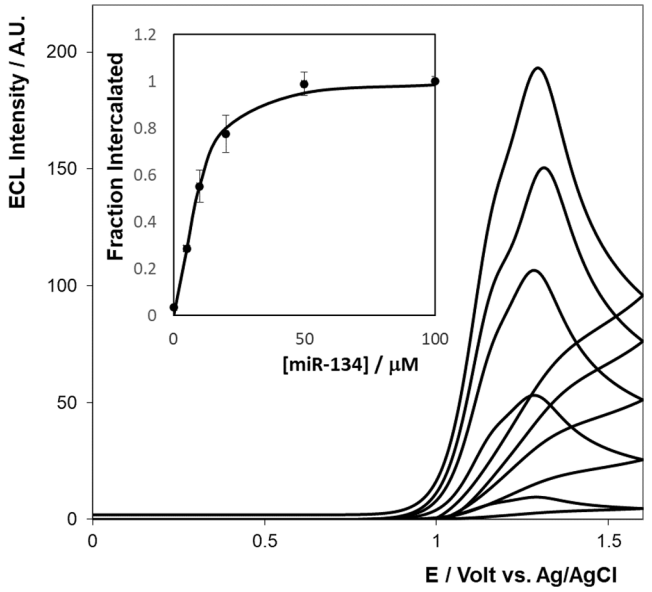

Fig. 5. ECL from a miR-134 capture-$[Ru(DPPZ)_2PIC]^{2+}$ monolayer in 1.0 M aqueous $LiClO_4$ containing 10 mM oxalate as co-reactant after exposure to solutions of miR-134 where the concentrations are (top to bottom) 100, 20, 10, 5 and 0.1 μM. The scan rate is 0.1 Vs^{-1}. The inset shows the dependence of the bound fraction on the miR-134 concentration where the solid points are the experimental data, and the solid line is the best fit to the Hill equation describing cooperative binding at n different binding sites.

$$\theta = \frac{K[miR-134]^n}{1+K[miR-134]^n} \quad (1)$$

where K is the association constant and n describes the number of binding sites. Non-linear generalized reduced gradient fitting in which both K and n are freely adjustable variables gives a high-quality fit (solid line in inset of Fig. 5) where K is 39 ± 3 and n is 1.70 ± 0.15. The number of binding sites is close to 2 which is consistent with cooperative binding involving two different sites or microenvironments with the capture strand-target duplex. It is not clear if these correspond to intercalation at different physical locations within the duplex due to the flexibility of the linker or if it is due to the capture strands being in different states, e.g., isolated vs. within dense RNA islands on the electrode surface. The association constant, 39 ± 3, corresponds to a free energy of −9.1 ± 0.2 kJ mol^{-1}. This value is significantly lower than that expected for this nucleic acid sequence, approximately −100 kJ mol^{-1}. Despite the relatively low surface coverage of the capture strands (approximately 35% of a close-packed monolayer), this weaker binding may suggest that the nucleic acids do not exist in aqueous environment but are within islands where the local coverage is higher decreasing the local dielectric constant and inhibiting hybridisation.

3.4. Analytical performance

From an analytical perspective, the inset of Fig. 5 shows that the ECL intensity increases linearly with increasing target concentration for 100 nM < [miR-134] less than 20 μM. The limit of detection could be further improved by increasing the binding strength, but this would of course reduce the dynamic range. Beyond analytical sensitivity, the impact of non-specific binding, NSB, e.g., of proteins present in blood, plasma and serum, is another major consideration. Fig. 6 shows the ECL response following hybridisation of a 50 μM solution of miR-134 and when the capture strands alone are exposed to 0.6 mM BSA (this matches the concentration of human serum albumin in blood). Significantly, the intensity of the ECL emission for the capture strands exposed to BSA, i.e., the negative control, shows less than 0.7% of the intensity observed for the duplex. This result suggests that protein, even if it does non-specifically adsorb, does not protect the excited state sufficiently from exposure to water to block non-radiative relaxation back to the ground state.

The impact of mismatches in the target on the ECL intensity has been investigated using 10 μM test solutions. A single base mismatch located in the middle of the target decreases I_{ECL} from 106 ± 5 A.U. for the fully complementary target to 32 ± 6 A.U. for the 1- base mismatch. Thus, while the sensor is not suitable for detecting single nucleotide polymorphisms, the discrimination even at the single base mismatch is acceptable. The ability to discriminate two base mismatches is excellent with I_{ECL} decreasing by 92% compared to the fully complementary miR-

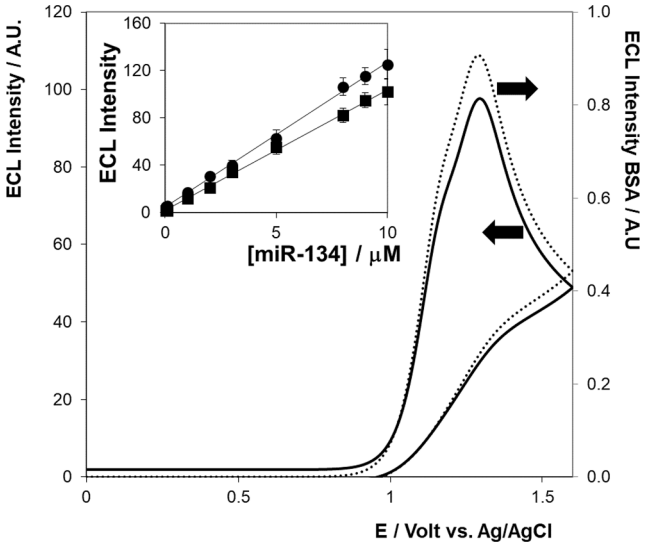

Fig. 6. Comparison of ECL response from a miR-134 Capture- $[Ru(dppz)_2PIC]^{2+}$ monolayer for 10 μM miR-134 (solid line, y-axis to the left) and 40 mM HSA (dashed line, y-axis to right). The inset shows the calibration in unprocessed human plasma that was first depleted of RNA and then spiked with the required miR-134 concentration. The circles (upper line, ECL intensity = 12.258 [miR-134] + 4.5879, R^2 = 0.9983) are the ECL intensities measured after the target has hybridised in plasma without any wash step while the squares (lower line, ECL intensity = 10.218 [miR-134] + 1.7754, R^2 = 0.9986) are the intensities obtained after a wash step.

134. However, it is also important to consider the selectivity over similar sequences that could actually be present in a blood plasma sample. miR-758 has a sequence of 12 bases that are the same as that found in miR-134 and is the most similar RNA to the fully complementary target likely to be found in real samples. Significantly, the ECL intensity for miR-758 is less than 3% of that found for the fully complementary target. These data indicate that the sensor is highly selective and capable of discriminating between the target and other miRNA that could be found within real samples.

To probe the real-world usefulness of the sensor developed we have investigated the performance in unprocessed human plasma. The inset of Fig. 6 shows a calibration curve in human plasma that has first been depleted of RNA and then spiked with different concentrations of the target. Significantly, the ECL intensities observed in serum are within 10% of those found in clean buffer. Fig. 6 shows that the dynamic range of the sensor is from 100 nM to 10 μM which compares favourably with that found in clean buffer (Fig. 5). The limit of detection, LOD, can be calculated using Equation (2):

$$LOD = 3.3^{*}\sigma/S \quad (2)$$

where σ is the standard deviation and S is the slope of the calibration curve. For this system the LOD is calculated to be 1×10^{-12} M (1 pM) and experiments using an actual 1 pM miR-134 solution given a measurable signal above the baseline.

A potential advantage of this assay format is that the need for wash cycles after the target has been hybridised may be reduced since the response is insensitive to the presence of protein and ECL requires the presence of a duplex. The inset of Fig. 6 reveals that the analytical sensitivity is approximately 17% higher before the wash step. However, the reproducibility without washing rivals that of the assay following a wash step suggesting that miR-134 concentrations can be measured in plasma without the absolute need for a wash step.

3.5. Detection of miR-134 in plasma from people with epilepsy

Plasma samples were obtained from healthy volunteers and from patients with temporal lobe epilepsy. The ECL intensity was measured in the unprocessed plasma using 10 mM oxalate as co-reactant and the results obtained are summarised in Table 1.

The healthy controls reveal miR-134 levels that are just above the LOD for the sensor while the epilepsy patients show significant variation with concentrations ranging from 100 nM to 1 μM. This variation may reflect the status of the patient on the day the samples were collected, e.g., the temporal proximity of a seizure. The data suggest that miR-134 is present at a higher concentration in people with epilepsy compared to healthy volunteers. These results are consistent with those found using qPCR and a complex centrifugal microfluidic device we reported previously.[26]

Table 1
Results for the electrochemiluminescent detection of miR-134 in unprocessed plasma samples.

Patient	Disease	I_{ECL}	[miR-134]
A	Healthy Control	1.8	less than5 pM
B	Healthy Control	1.8	less than5 pM
C	TLE	12.4	100 nM
D	TLE	2.8	120 nM
E	TLE	3.1	150 nM
F	TLE	3.4	1050 nM

4. Conclusions

We have demonstrated a simplified, electrochemiluminescent sensor for the detection of a miRNA associated with epilepsy. The sensor has excellent ability to discriminate against structurally related miRNAs and responds only very weakly to a two-base mismatch. The ECL intensity is not significantly affected by the presence of proteins such as BSA indicating that protein does not protect the excited state of the $[Ru(DPPZ)_2PIC]^2$ dye from radiationless quenching by water. This lack of sensitivity to the presence of protein is reflected when measuring miR-134 in unprocessed plasma where the assay results are highly reproducible even when a wash step is not carried out. The miR-134 concentrations in healthy volunteers and people with temporal lobe epilepsy can be easily distinguished. Moreover, we have shown that the absolute concentration of miR-134 varies significantly between epilepsy patients (by a factor of approximately 10) which may open the possibility of using a panel of miRNA for early diagnosis of epilepsy, the monitoring of disease state, compliance with medication and perhaps ultimately, to predict impending seizures. Electrochemiluminescence is well placed to deliver a low-density array since it can be multiplexed either by changing the metal complex structure so that ECL is turned on at different potentials, e.g., by changing the identity of the metal centre, or tuning the emission wavelength, e.g., by changing the peripheral ligands.

Declaration of Competing Interest

The authors declare that they have no known competing financial interests or personal relationships that could have appeared to influence the work reported in this paper.

Acknowledgement

This publication has emanated from research supported in part by a research grant from Science Foundation Ireland (SFI) under Grant Number 16/RC/3948 and co-funded under the European Regional Development Fund and by FutureNeuro industry partners.

References

[1] O. Devinsky, A. Vezzani, T. O'Brien, N. Jette, I.E. Scheffer, M. de Curtis, P. Perucca, Epilepsy, Nat. Rev. Dis. Primers 4 (2018) 18024.
[2] C. Chang, C.-M. Chang, W.-H. Chang, C.-H. Wang, J.-H. Wang, J.D. Maid, G.B. Lee, Nucleic acid amplification using microfluidic systems, Lab Chip 13 (2013) 1225.
[3] L. Wei, H. Boutouil, R.R. Gerbatin, O. Mamad, M. Heiland, C.R. Reschke, F. Del Gallo, P.F. Fabene, D.C. Henshall, M. Lowery, G. Morris, C. Mooney, Detection of spontaneous seizures in EEGs in multiple experimental mouse models of epilepsy, J. Neur. Eng. 18 (5) (2021), 056060.
[4] G. Liu, R. Xiao, L. Xu, J. Cai, Minireview of Epilepsy Detection Techniques Based on Electroencephalogram Signals, Front. Sys. Neurosci. 15 (2021), 685387.
[5] D. Guery, S. Rheims, Clinical Management of Drug Resistant Epilepsy: A Review on Current Strategies, Neuropsychiatr. Dis. Treat. 17 (2021) 2229.
[6] A. Kenny, H. McArdle, M. Calero, A. Rabano, S.F. Madden, K. Adamson, R. J. Forster, E. Spain, J.H.M. Prehn, D.C. Henshall, M. Medina, E.M. Jimenez-Mateos, T. Engel, Elevated Plasma microRNA-206 Levels Predict Cognitive Decline and Progression to Dementia from Mild Cognitive Impairment, Biomolecules 11 (2019) 734.
[7] G. Morris, D. O'Brien, D.C. Henshall, Opportunities and challenges for microRNA-targeting therapeutics for epilepsy, *Tr*, Pharm. Sci. 42 (7) (2021) 605–616.
[8] M. Simonato, D.V. Agoston, A. Brooks-Kayal, C. Dulla, B. Fureman, Identification of clinically relevant biomarkers of epileptogenesis—a strategic roadmap, Nat. Rev. Neurol. 17 (4) (2021) 231.
[9] R. Raoof, S. Bauer, H. El Naggar, N.M.C. Connolly, G.P. Brennan, E. Brindley, T. Hill, H. McArdle, E. Spain, R.J. Forster, J.H.M. Prehn, H. Hamer, N. Delanty, F. Rosenow, C. Mooney, D.C. Henshall, Dual-center, dual-platform microRNA profiling identifies potential plasma biomarkers of adult temporal lobe epilepsy, EBioMedicine 38 (2018) 127–141.
[10] D.C. Henshall, MicroRNA and epilepsy: profiling, functions and potential clinical applications, Curr. Opin. Neurol. 27 (2014) 199.
[11] R. Fiore, S. Khudayberdiev, M. Christensen, G. Siegel, S.W. Flavell, T.-K. Kim, M. E. Greenberg, G. Schratt, Mef2-mediated transcription of the miR379-410 cluster regulates activity-dependent dendritogenesis by fine-tuning Pumilio2 protein levels, EMBO J. 28 (2009) 697.
[12] G.M. Schratt, F. Tuebing, E.A. Nigh, C.G. Kane, M.E. Sabatini, M. Kiebler, M. E. Greenberg, A brain-specific microRNA regulates dendritic spine development, Nature 439 (7074) (2006) 283–289.
[13] J. Peng, A. Omran, M. Usman Ashhab, H. Kong, N. Gan, F. He, F.Y. Peng, Expression Patterns of miR-124, miR-134, miR-132, and miR-21 in an Immature Rat Model and Children with Mesial Temporal Lobe Epilepsy, J. Mol. Neurosci. 50 (2013) 291.
[14] E.M. Jimenez-Mateos, T. Engel, P. Merino-Serrais, R.C. McKiernan, K. Tanaka, G. Mouri, T. Sano, C. O'Tuathaigh, J.L. Waddington, S. Prenter, N. Delanty, M.

A. Farrell, D.F. O'Brien, R.M. Conroy, R.L. Stallings, J. DeFelipe, D.C. Henshall, C Henshall Silencing microRNA-134 produces neuroprotective and prolonged seizure-suppressive effects, Nat. Med. 18 (7) (2012) 1087–1094.
[15] P. Roncon, M. Soukupovà, A. Binaschi, C. Falcicchia, S. Zucchini, M. Ferracin, S. R. Langley, E. Petretto, M.R. Johnson, G. Marucci, R. Michelucci, G. Rubboli, M. Simonato, MicroRNA profiles in hippocampal granule cells and plasma of rats with pilocarpine-induced epilepsy - comparison with human epileptic samples, Sci. Rep. 5 (2016) 14143.
[16] R. Surges, A. Kretschmann, K. Abnaof, M. van Rikxoort, K. Ridder, H. Fröhlich, B. Danis, R.M. Kaminsk, P. Foerch, C.E. Elger, F. Weinsberg, A. Pfeifer, Changes in serum miRNAs following generalized convulsive seizures in human mesial temporal lobe epilepsy, Biochem. Biophys. Res. Commun. 481 (2016) 13.
[17] A. Campbell, G. Morris, J.P. Heller, E. Langa, E. Brindley, J. Worm, M.A. Jensen, Meghan T Miller, David C Henshall, Cristina R Reschke, Antagomir-mediated suppression of microRNA-134 reduces kainic acid-induced seizures in immature mice, Sci. Rep. 11 (1) (2021) 1.
[18] D.C. Henshall, Epigenetics and noncoding RNA: Recent developments and future therapeutic opportunities, Euro. *J. Paed. Neurol.* 24 (2020) 30.
[19] J.F. Rusling, R.J. Forster, Biosensors designed for clinical applications, Biomedicines 9 (7) (2021) 702.
[20] E. Spain, T.E. Keyes, R.J. Forster, DNA sensor based on vapour polymerised PEDOT films functionalised with gold nanoparticles, Biosens. Bioelec. 41 (2016) 65.
[21] E. Spain, K. Adamson, M. Elshahawy, I. Bray, T.E. Keyes, R.L. Stallings, R.J. Forster, Hemispherical platinum: silver core: shell nanoparticles for miRNA detection, Analyst 142 (5) (2017) 752.
[22] E. Spain, E.M. Jimenez-Mateos, R. Raoof, H. ElNaggar, N. Delanty, R.J. Forster, D. C. Henshall, Direct, non-amplified detection of microRNA-134 in plasma from epilepsy patients, RSC Adv. 5 (109) (2015) 90071–90078.
[23] E. Spain, E. Brennan, T.E. Keyes, R.J. Forster, Dual function metal nanoparticles: Electrocatalysis and DNA capture, Electrochim. Acta 128 (2014) 61–66.
[24] E. Spain, A. McCooey, C. Dolan, H. Bagshaw, N. Leddy, T.E. Keyes, R.J. Forster, Electrodeposited gold–copper core–shell nanowires for high sensitivity DNA detection, Analyst 139 (21) (2014) 5504–5508.
[25] E. Spain, A. McCooey, K. Joyce, T.E. Keyes, R.J. Forster, Gold nanowires and nanotubes for high sensitivity detection of pathogen DNA, Sens. and Actuat. B 215 (2015) 159–165.
[26] H. McArdle, E.M. Jimenez-Mateos, R. Raoof, E. Carthy, D. Boyle, H. El Naggar, N. Delanty, H. Hamer, M. Dogan, T. Huchtemann, P. Körtvelyessy, F. Rosenow, R. J. Forster, D.C. Henshall, E. Spain, "TORNADO" – Theranostic One-Step RNA Detector; microfluidic disc for the direct detection of microRNA-134 in plasma and cerebrospinal fluid, Sci. Rep. 7 (2017) 1750.
[27] P. Bertoncello, P. Ugo, Recent Advances in Electrochemiluminescence with Quantum Dots and Arrays of Nanoelectrodes, ChemElectroChem 4 (7) (2017) 1663–1676.
[28] P. Bertoncello, A.J. Stewart, L. Dennany, Analytical applications of nanomaterials in electrogenerated chemiluminescence, Anal. Bioanal. Chem. 406 (23) (2014) 5573.
[29] N. Sojic, Analytical Electrogenerated Chemiluminescence, Detection Science; Royal Society of Chemistry: Cambridge, **2019**.
[30] F. Liu, F. Du, F. Yuan, S. Quan, Y. Guan, G. Xu, Electrochemiluminescence bioassays based on carbon nitride nanomaterials and 2D transition metal carbides, Curr. Opinion in Electrochem. 34 (2022) 100981.
[31] R. J. Forster, ECL of Nanomaterials: Novel Materials, Detection Strategies and Applications, Analytical Electrogenerated Chemiluminescence: From Fundamentals to Bioassays; Sojic, N., Ed. **2019**, 247.
[32] G. Valenti, A. Fiorani, H. Li, N. Sojic, F. Paolucci, Essential Role of Electrode Materials in Electrochemiluminescence Applications, ChemElectroChem 3 (12) (2016) 1990–1997.
[33] A. Devadoss, A.-M. Spehar-Délèze, D.A. Tanner, P. Bertoncello, R. Marthi, T. E. Keyes, R.J. Forster, Enhanced electrochemiluminescence and charge transport through films of metallopolymer-gold nanoparticle composites, Langmuir 26 (3) (2010) 2130–2135.
[34] L. Cumba, Y. Pellegrin, F. Melinato, R.J. Forster, Enhanced Electrochemiluminescence from 3D Nanocavity Electrode Arrays, Sens. and Act. Rep. 4 (2022) 100082.
[35] S.F. Douman, M. Ruiz De Eguilaz, L.R. Cumba, S. Beirne, G.G. Wallace, Z. Yue, E. I. Iwuoha, R.J. Forster, Electrochemiluminescence at 3D Printed Titanium Electrodes, Front. Chem. 9 (2021) 279.
[36] S.F. Douman, D. Collins, L.R. Cumba, S. Beirne, G.G. Wallace, Z. Yue, E.I. Iwuoha, F. Melinato, Y. Pellegrin, R.J. Forster, Wireless electrochemiluminescence at functionalised gold microparticles using 3D titanium electrode arrays, Chem. Commun. 57 (38) (2021) 642.
[37] S.F. Douman, E. Brennan, E.I. Iwuoha, R.J. Forster, Wireless Electrochemiluminescence at Nafion-Carbon Microparticle Composite Films, Anal. Chem. 89 (21) (2017) 11614.
[38] T. Joshi, G.J. Barbante, P.S. Francis, C.F. Hogan, A.M. Bond, G. Gasser, L. Spiccia, Electrochemiluminescent Monomers for Solid Support Syntheses of Ru(II)-PNA Bioconjugates: Multimodal Biosensing Tools with Enhanced Duplex Stability, Inorg. Chem. 51 (5) (2012) 3302.
[39] T. Joshi, G.J. Barbante, P.S. Francis, C.F. Hogan, A.M. Bond, L. Spiccia, Electrochemiluminescent Peptide Nucleic Acid-Like Monomers Containing Ru(II)–Dipyridoquinoxaline and Ru(II)–Dipyridophenazine Complexes, Inorg. Chem. 50 (23) (2011) 12172.
[40] R.-F. Huang, H.-X. Liu, Q.-Q. Gai, G.-J. Liu, Z. Wei, A facile and sensitive electrochemiluminescence biosensor for Hg^{2+} analysis based on a dual-function oligonucleotide probe, Biosens. Bioelec. 71 (2015) 194–199.
[41] L. Hu, Z. Bian, H. Li, S. Han, Y. Yuan, L. Gao, G. Xu, Ru(bpy)2d ppz]2+ Electrochemiluminescence Switch and Its Applications for DNA Interaction Study and Label-free ATP Aptasensor, Anal. Chem. 81 (23) (2009) 9807.
[42] H. Liu, X. Zhou, W. Liu, X. Yang, D. Xing, Paper-Based Bipolar Electrode Electrochemiluminescence Switch for Label-Free and Sensitive Genetic Detection of Pathogenic Bacteria, Anal. Chem. 88 (20) (2016) 10191.
[43] H. Wang, Y. Yuan, Y. Zhuo, Y. Chai, R. Yuan, Sensitive Electrochemiluminescence Immunosensor for Detection of N-Acetyl-β-d-glucosaminidase Based on a "Light-Switch" Molecule Combined with DNA Dendrimer, Anal. Chem. 88 (11) (2016) 5797.
[44] H. Liu, X. Zhou, Q. Shen, D. Xing, Paper-based electrochemiluminescence sensor for highly sensitive detection of amyloid-β oligomerization: Toward potential diagnosis of Alzheimer's disease, Theranostics. 8 (8) (2018) 2289–2299.
[45] T. Zhou, R. Huang, M. Huang, J. Shen, Y. Shan, D. Xing, CRISPR/Cas13a Powered Portable Electrochemiluminescence Chip for Ultrasensitive and Specific MiRNA Detection, Adv. Sci. 7 (2020) 1903661.
[46] Y. Nie, X. Yuan, P. Zhang, Y.-Q. Chai, R. Yuan, Versatile and Ultrasensitive Electrochemiluminescence Biosensor for Biomarker Detection Based on Nonenzymatic Amplification and Aptamer-Triggered Emitter Release, Anal. Chem. 91 (5) (2019) 3452.
[47] R. Huang, L.-R. Wang, L.-H. Guo, Highly sensitive electrochemiluminescence displacement method for the study of DNA/small molecule binding interactions, Anal. Chim. Acta 676 (1-2) (2010) 41–45.
[48] R.J. Forster, Heterogeneous Kinetics of Metal-and Ligand-Based Redox Reactions within Adsorbed Monolayers, Inorg. Chem. 35 (1996) 3394.
[49] L. Cosgrave, M. Devocelle, R.J. Forster, T.E. Keyes, Multimodal cell imaging by ruthenium polypyridyl labelled cell penetrating peptides, Chem. Commun. 46 (1) (2010) 103–105.
[50] H.H. Cheng, H.S. Yi, Y. Kim, E.M. Kroh, J.W. Chien, K.D. Eaton, M.T. Goodman, J. F. Tait, M. Tewari, C.C. Pritchard, S. Kiechl, Plasma Processing Conditions Substantially Influence Circulating microRNA Biomarker Levels, PLoS One 8 (6) (2013) e64795.
[51] E. Laviron, Surface linear potential sweep voltammetry: Equation of the peaks for a reversible reaction when interactions between the adsorbed molecules are taken into account, J. Electroanal. Chem. 52 (3) (1974) 395–402.
[52] A.P. Brown, F.C. Anson, Cyclic and differential pulse voltammetric behavior of reactants confined to the electrode surface, Anal. Chem. 49 (1977) 1589.
[53] P. Bertoncello, E.T. Kefalas, Z. Pikramenou, P.R. Unwin, R.J. Forster, Adsorption Dynamics and Electrochemical and Photophysical Properties of Thiolated Ruthenium 2,2′-Bipyridine Monolayers, J. Phys. Chem. B 110 (20) (2006) 10063–10069.